

Single-Molecule Study on Polymer Diffusion in a Melt State: Effect of Chain Topology

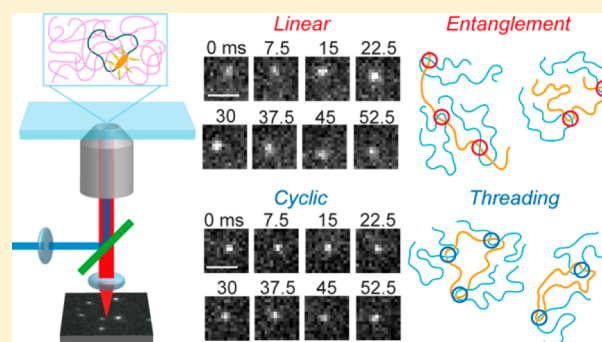
Satoshi Habuchi,^{*,†} Susumu Fujiwara,[‡] Takuya Yamamoto,[‡] Martin Vacha,[‡] and Yasuyuki Tezuka^{*,‡}

[†]Biological and Environmental Sciences and Engineering Division, King Abdullah University of Science and Technology, P.O. Box 4700 KAUST, Thuwal 23955-6900, Kingdom of Saudi Arabia

[‡]Department of Organic and Polymeric Materials, Tokyo Institute of Technology, 2-12-1 O-okayama, Meguro-ku, Tokyo 152-8552, Japan

S Supporting Information

ABSTRACT: We report a new methodology for studying diffusion of individual polymer chains in a melt state, with special emphasis on the effect of chain topology. A perylene diimide fluorophore was incorporated into the linear and cyclic poly-(THF)s, and real-time diffusion behavior of individual chains in a melt of linear poly(THF) was measured by means of a single-molecule fluorescence imaging technique. The combination of mean squared displacement (MSD) and cumulative distribution function (CDF) analysis demonstrated the broad distribution of diffusion coefficient of both the linear and cyclic polymer chains in the melt state. This indicates the presence of spatiotemporal heterogeneity of the polymer diffusion which occurs at much larger time and length scales than those expected from the current polymer physics theory. We further demonstrated that the cyclic chains showed marginally slower diffusion in comparison with the linear counterparts, to suggest the effective suppression of the translocation through the threading-entanglement with the linear matrix chains. This coincides with the higher activation energy for the diffusion of the cyclic chains than of the linear chains. These results suggest that the single-molecule imaging technique provides a powerful tool to analyze complicated polymer dynamics and contributes to the molecular level understanding of the chain interaction.



Single-molecule fluorescence microscopy has been revealing static and dynamic disorders in a variety of complex systems in chemistry, physics, and biology.¹ In particular, single-molecule microscopy is a powerful tool to investigate nanoscale heterogeneities and their relationship with molecular movements in many systems^{2,3} as ensemble-averaged experimental methods do not provide direct information about motions of individual molecules.⁴

Viscoelastic properties of polymers have been studied for decades by means of ensemble-averaged methods such as light scattering, NMR, and viscosity measurement.^{5–7} Although polymer physics theories have been developed based on the findings of the ensemble experiments, molecular level understanding of the polymer dynamics is still a challenging task since the dynamics of individual polymer chains cannot be visualized by those methods. In fact, single-molecule studies have suggested the presence of large spatial and temporal heterogeneity of the polymer dynamics.^{8–13} For instance, spatial heterogeneities of the local polymer chain dynamics in thin films near glass transition temperatures were suggested by the single-molecule imaging experiment.⁹ Such the observation cannot be fully explained by the polymer physics theory developed based on the ensemble methods.

Diffusion process of polymers is one of the important research fields in polymer physics as this influences polymer processing and fabrication of plastic, films, and fibers.¹⁴ The static and dynamic properties of entangled polymer chains in a semidilute solution or in a melt have often been described by the reptation model.^{15–18} In this model, an entangled polymer diffuses in a dynamic tube confined by neighboring chains, and therefore, the chain ends play a dominant role. The reptation model has been applied to describe the diffusion of linear polymers.^{19–21}

In contrast, diffusion of cyclic polymers should be described by distinct mechanisms since they have no chain ends. An amoeba-like motion has been suggested theoretically for the diffusion mechanism of cyclic polymers.²² Simulation works have suggested more compact conformation and less interpenetration of cyclic polymers in the melt state, which leads to faster diffusion of the cyclic polymers.^{23–25} On the other hand, experimental studies reported inconsistent results on the diffusion coefficients (D) of the cyclic and linear polymer melts.^{26–28} Furthermore, dynamics of a blend of linear and

Received: April 27, 2013

Accepted: July 1, 2013

Published: July 1, 2013



cyclic polymers are suggested to be very different from the average properties of the two components.^{29,30} It has been demonstrated that even trace amounts of the linear chains in the cyclic polymer melt alters a rheological response significantly.³¹ Several theoretical models have been proposed to describe the dynamic properties of the blends of the linear and cyclic polymer melts.³² Despite a large number of experimental,^{33–39} theoretical,^{40,41} and simulation studies,^{42,43} the molecular mechanism of cyclic polymer dynamics remains elusive. This is partly due to the intrinsic heterogeneity that the solution and melt of topological polymers possess. The heterogeneity makes molecular level understanding of polymer dynamics especially difficult by means of ensemble-averaged experimental methods.

Single-molecule fluorescence imaging of the diffusion behavior of linear and branched polymers has been performed by incorporating a fluorophore into the polymer chains.^{19,29,44} Polymer dynamics have also been studied at the single-molecule level by embedding fluorescent probe molecules in the polymer matrix. However, this approach provides indirect information about chain dynamics. Obviously, a fluorophore incorporating polymer can provide more direct information about the chain dynamics.^{45–47} We previously reported real-time imaging of the diffusion of synthetic linear and cyclic polymers at the single-molecule level in a semidilute polymer solution, by employing the linear (1) and cyclic (2) poly(tetrahydrofuran)s (poly(THF)s) containing a perylene diimide unit as a fluorophore (Figure 1).⁴⁸ The single-molecule

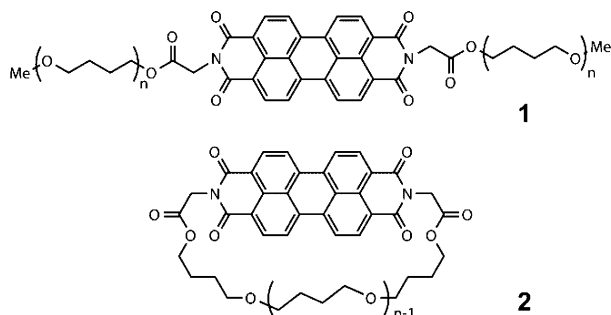


Figure 1. Linear (1) and cyclic (2) poly(THF) molecules containing a perylene diimide moiety.

experiment revealed a hidden multimode diffusion of the cyclic polymer molecules which is in contrast to the homogeneous diffusion of the linear polymer molecules. The result suggested the presence of threaded and unthreaded cyclic polymer chains with the matrix linear chains, in which the former slow down the diffusion of the cyclic polymer chains. The study demonstrated that single-molecule experiments can indeed unravel heterogeneity in the polymer dynamics, which is the important step toward molecular level understanding of the complicated cyclic polymer dynamics.⁴⁹

In the present study, we report the single-molecule diffusion of the cyclic (2) and linear (1) polymers in the melt state. As compared with the threading effect that we previously found in the semidilute solution,⁴⁸ the entanglement and threading of the cyclic polymer molecules in the melt are more relevant to the previous experimental, theoretical, and simulation studies. Therefore, we should be able to obtain deeper insights in any topology effects on the diffusion process by cyclic polymers against linear counterparts. We demonstrate broad distributions of the diffusion coefficient of the polymer chains in the melts

and the effect of topology on the chain interaction in the polymer melts.

EXPERIMENTAL SECTION

Materials. 1 and 2 were synthesized by means of an electrostatic self-assembly and covalent fixation process, which is reported elsewhere.^{48,50–52} Molecular weights of 1 and 2 are $M_n = 4200$ ($M_w/M_n = 1.12$) and $M_n = 3800$ ($M_w/M_n = 1.19$), respectively. The polymer chains of 1 and 2 consist, on average, of 240 and 250 atoms, respectively. The gyration radii of 1 and 2 are 2.4 and 1.6 nm (see the Supporting Information). For single-molecule fluorescence imaging experiments, a melt of unlabeled linear poly(THF) (Aldrich, $M_n = 3000$, $M_w/M_n = 1.89$) and a chloroform solution of 1 or 2 (10^{-6} M) were mixed at the volume ratio of 99 to 1. The solvent was evaporated completely by heating the mixture. The mole fraction of 1 and 2 in the melt samples was 32–35 ppb. A 10 μ L volume of the sample was sandwiched between two microscope coverslips, resulting in the sample thickness of 10 μ m. Note that we were not able to use cyclic poly(THF) as a matrix polymer due to a high fluorescence background from impurities.

Single-Molecule Fluorescence Imaging Experiment. Fluorescence images were recorded using an inverted microscope (Olympus, IX71) equipped with a high N.A. objective lens (Olympus, $\times 100$, N.A. = 1.3) (Figure 2). The sample

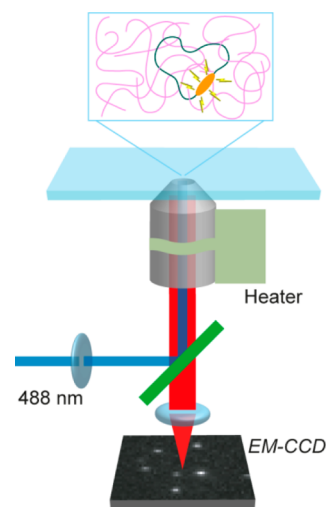


Figure 2. Schematic illustration of the experimental setup.

temperature was controlled using an objective heater (Biotech; temperature range, ambient to 333 K; temperature stability, ± 0.2 °C). The sample was set on the stage of the microscope and kept at a constant temperature (292, 303, or 313 K) for 1 h before recording the fluorescence images. This ensures that the sample has reached the equilibrium condition. A 488 nm line from a CW Ar–Kr ion laser (Coherent Innova 70C) was used for excitation. A circularly polarized light was obtained by using a Berek compensator (Newport) and introduced into the microscope through an excitation filter (Semrock, LL01-488-12.5) and the objective. An illuminated area was about 20 μ m in diameter. The excitation power of the 488 nm light was 2.3 kW cm^{-2} . The fluorescence signal was corrected by the same objective, passed through a dichroic mirror (Omega optical, 500DRLP) and an emission filter (Semrock, BLP01–488R-25), and was focused on an EM-CCD camera (Andor technology, iXon^{EM+}). The fluorescence images

were recorded with a 7.5 ms exposure time. The pixel size of the images was 160 nm. More than 200 single-molecule diffusion trajectories were recorded in each experimental condition.

Image Analysis. The diffusion of **1** and **2** was analyzed by means of single-molecule tracking analysis. We analyzed 232 and 421 trajectories for **1** at 303 and 313 K, respectively. We analyzed 562 and 222 trajectories for **2** at 303 and 313 K, respectively. The positions of the molecules in each image were determined by using two-dimensional Gaussian fitting using routines written in Matlab^{53,54}

$$z = z_0 + A \exp\left[-\frac{(x - x_c)^2}{2w_x^2}\right] \exp\left[-\frac{(y - y_c)^2}{2w_y^2}\right] \quad (1)$$

where x_c and y_c are the centroid position along the x and y axes, respectively. A and z_0 are a Gaussian height and an offset, respectively. w_x and w_y are the widths of the Gaussian along the x and y axes, respectively.

RESULTS AND DISCUSSION

Visualization of Diffusional Motion of Single Polymer Chains in Melts. We measured fluorescence images of **1** and **2** in the linear poly(THF) matrix at a temperature in the range of 293–313 K. A melting temperature of the linear poly(THF) was determined to be 299 K by differential scanning calorimetry (data not shown). Note that the glass transition temperature (T_g) of poly(THF) ($T_g = 189$ K) is far below the temperature range of the experiment. At 293 K, the diffusional motion in some area was completely blocked, while the slow diffusional motion was observed in other areas (see Supporting Information). In contrast, **1** and **2** displayed much faster diffusion in all area recorded when the fluorescence images were measured at 303 and 313 K (see the Supporting Information). Those results confirm that diffusion of **1** and **2** in the melt of linear poly(THF) can be measured at the single-molecule level.

Analysis of the Diffusion Modes in the Polymer Melts.

The top panels in Figure 3 show the time-course of single-molecule fluorescence images of diffusing **1** (Figure 3a,c) and **2** (Figure 3b,d) in the melt of the linear poly(THF) matrix recorded at 303 (Figure 3a,b) and 313 K (Figure 3c,d). The position of the molecule in each image was determined by a two-dimensional Gaussian fitting of the image (see the Experimental Section). Examples of the obtained diffusion trajectories are shown in the bottom panels in Figure 3. The D values of individual molecules were determined by mean squared displacement (MSD) analysis of the trajectories using an equation

$$\text{MSD}(\Delta t) = \langle (x_{i+n} - x_i)^2 + (y_{i+n} - y_i)^2 \rangle \quad (2)$$

where x_i and y_i are the positions of the molecule in the image frame i , and n denotes the frame number with the time lapse Δt from frame i . The D value was determined by the initial slope of the equation

$$\text{MSD}(\Delta t) = 4D\Delta t \quad (3)$$

and plotted in frequency histograms (Figure 4, blue bars).

In order to estimate statistical errors of the MSD analysis which is due to a limited number of measured locations in each diffusion trajectory, we calculated the statistical probability

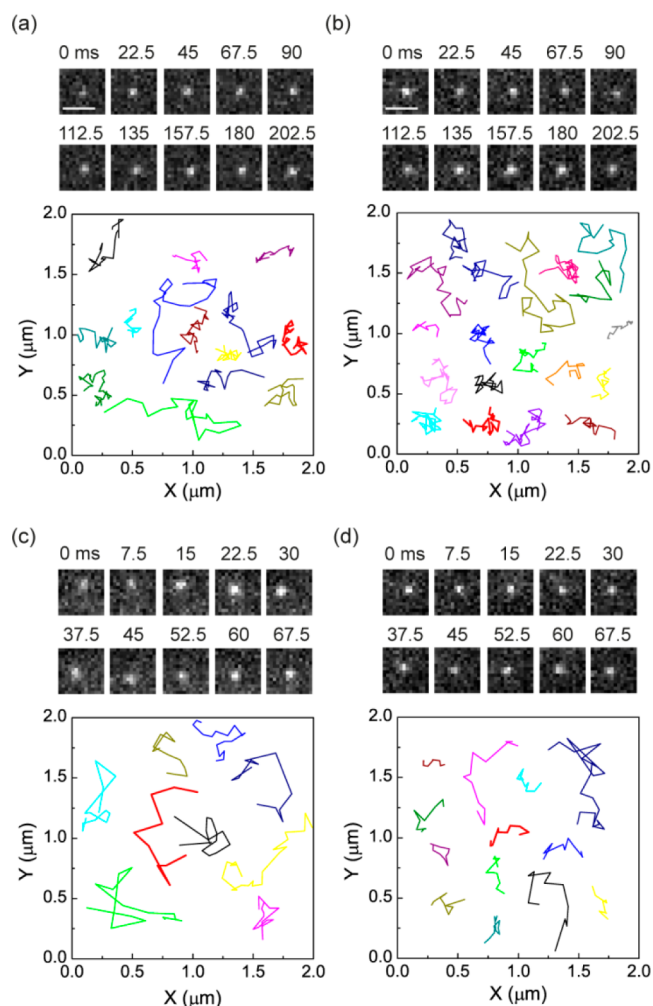


Figure 3. (top) Single-molecule fluorescence images of diffusion. (a, c) **1** and (b, d) **2** each mixed with linear poly(THF) melt. Scale bar = 1 μm . (bottom) Single-molecule diffusion trajectories of diffusing molecules of (a) **1** at 303 K, (b) **2** at 303 K, (c) **1** at 313 K, and (d) **2** at 313 K. The red trajectories correspond to the fluorescence images displayed in the top panels.

distribution of D in a homogeneous environment (Figure 3, black lines),^{55,56}

$$p(D) dD = \frac{1}{(N-1)!} \left(\frac{N}{D_0}\right)^N D^{N-1} \exp\left(-\frac{ND}{D_0}\right) dD \quad (4)$$

where N is the number of independent pairs (number of displacements), D_0 is the true mean diffusion coefficient, and D is the experimental diffusion coefficient for an individual trajectory. The median of D values in the respective histograms were used as an estimate for D_0 . Note that the medians are used in the analysis since the mean values are influenced significantly by the small number of fluorescent impurity molecules which diffuse much faster than **1** and **2**. For this analysis, the experimentally obtained trajectories were all cut such that they contained 10 data points (number of displacements). Any deviation from the theoretically calculated distributions suggests the heterogeneity in the diffusion. Figure 4 clearly shows the deviations between the experimentally determined D value histograms (Figure 4, blue bars) and theoretically calculated distributions (Figure 4, black lines), suggesting inhomogeneous diffusion of both **1** and **2** in the melt state.

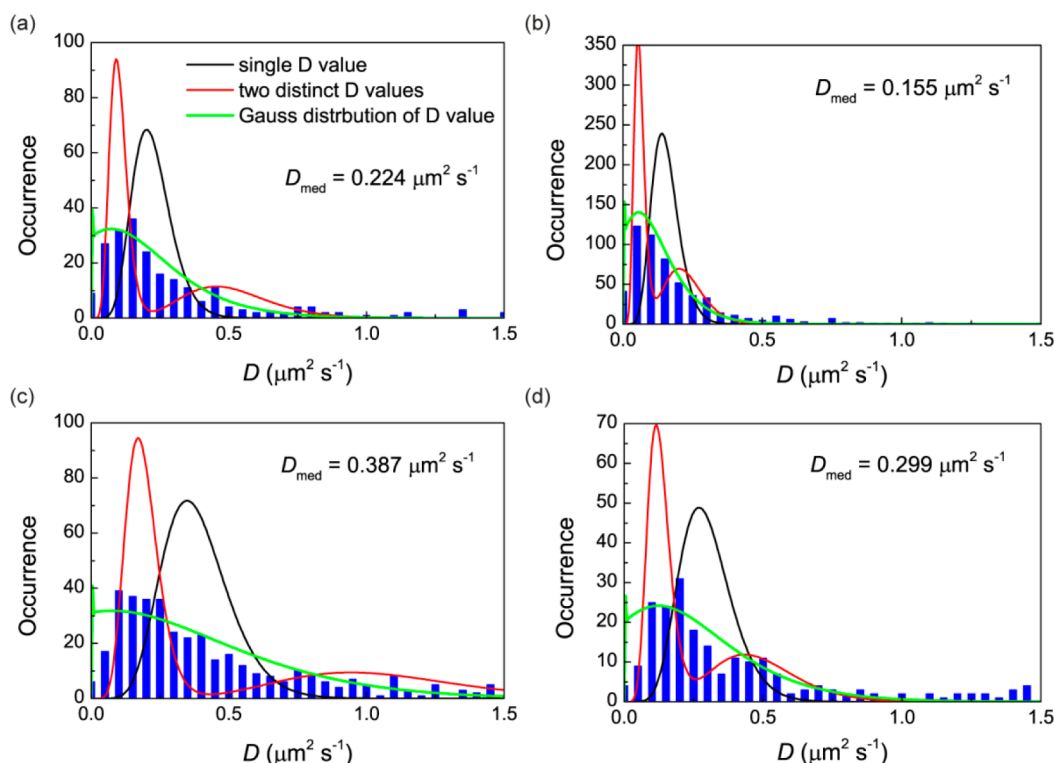


Figure 4. Frequency histograms (blue bars) of the diffusion coefficient determined for (a) **1** at 303 K, (b) **2** at 303 K, (c) **1** at 313 K, and (d) **2** at 313 K each mixed with linear poly(THF) melt. The solid lines show theoretical statistical distributions of the diffusion coefficient calculated based on three different diffusion models: diffusion in a homogeneous environment with the diffusion coefficient given by the medians of the respective histograms (black lines), two distinct diffusion modes with the diffusion coefficients and their relative amplitudes determined by double-exponential fitting of the cumulative distribution functions (red lines), and broad distribution of the diffusion coefficient which is determined by the fitting of the cumulative distribution functions with eq 7 (green lines).

The diffusion trajectories were further analyzed using a cumulative distribution function (CDF), $P(r^2, i\Delta t)$, which is the cumulative probability of finding the diffusing molecule within a radius r from the origin at time lag $i\Delta t$.⁵⁷

$$P(r^2, i\Delta t) = \int_0^r (r'^2, i\Delta t) dr' \\ = 1 - \sum_{i=0}^n \left\{ A_i \exp \left[-\frac{r^2}{4D_i(i\Delta t)} \right] \right\} \quad (5)$$

where A_i is the fraction of the component i . If the CDF displays a multiexponential behavior, this suggests the presence of multiple diffusion modes in the sample. The CDFs clearly show multiexponential behavior for both **1** and **2** at both 303 K and 313 K (Figure 5, left panels). The multiexponential behavior of the CDFs (Figure 5, left panels) together with the marked deviations between the experimentally determined D value histograms and theoretically calculated distributions suggest the presence of multiple diffusion modes in both **1** and **2**. This result is in contrast to the homogeneous diffusion of **1** in the semidilute solution of linear poly(THF) observed previously.⁴⁸

Analysis of the Multiple Diffusion Modes in the Polymer Melts. To facilitate comparison with diffusion of **1** and **2** in a semidilute solution in which two distinct diffusion components have been observed, we attempted to fit the obtained CDFs with double-exponential functions. Using the double-exponential fitting, two D values were obtained for each sample (see the Supporting Information). The statistical probability distribution of D in dual mode diffusion was calculated using an equation

$$p(D) dD = \frac{A_1}{(N-1)!} \left(\frac{N}{D_{01}} \right)^N D^{N-1} \exp \left(\frac{-ND}{D_{01}} \right) dD \\ + \frac{A_2}{(N-1)!} \left(\frac{N}{D_{02}} \right)^N D^{N-1} \exp \left(\frac{-ND}{D_{02}} \right) dD \quad (6)$$

where D_{01} and D_{02} are the diffusion coefficients of two diffusion modes determined by the CDF analysis, and A_1 and A_2 are the fraction of each diffusion component estimated from the CDF analysis. The calculated distributions are displayed in Figure 4 (red lines). Although the double-exponential decaying functions fit the CDFs well, the statistical probability distributions of the D values calculated based on the obtained two diffusion components do not reproduce the experimentally determined D value histograms. This is in contrast to a bimodal distribution in the D value histogram with a corresponding double-exponential decay of the CDF observed for the diffusion of **2** in the semidilute solution in the previous study,⁴⁸ in which the two D values obtained from the CDF analysis coincided with the peaks in the D histogram. In this study, while the two D values were obtained from the CDF analysis in each melt sample (see the Supporting Information), the frequency histograms of D do not show any sign of bimodal distribution with the peak values corresponding to these D values (Figure 4). These findings suggest the broad distribution of D in both **1** and **2** in the melt of linear poly(THF) rather than the presence of two distinct diffusion components.

Distribution of Diffusion Coefficients in the Polymer Melts. Instead of analyzing the CDFs with distinct diffusion

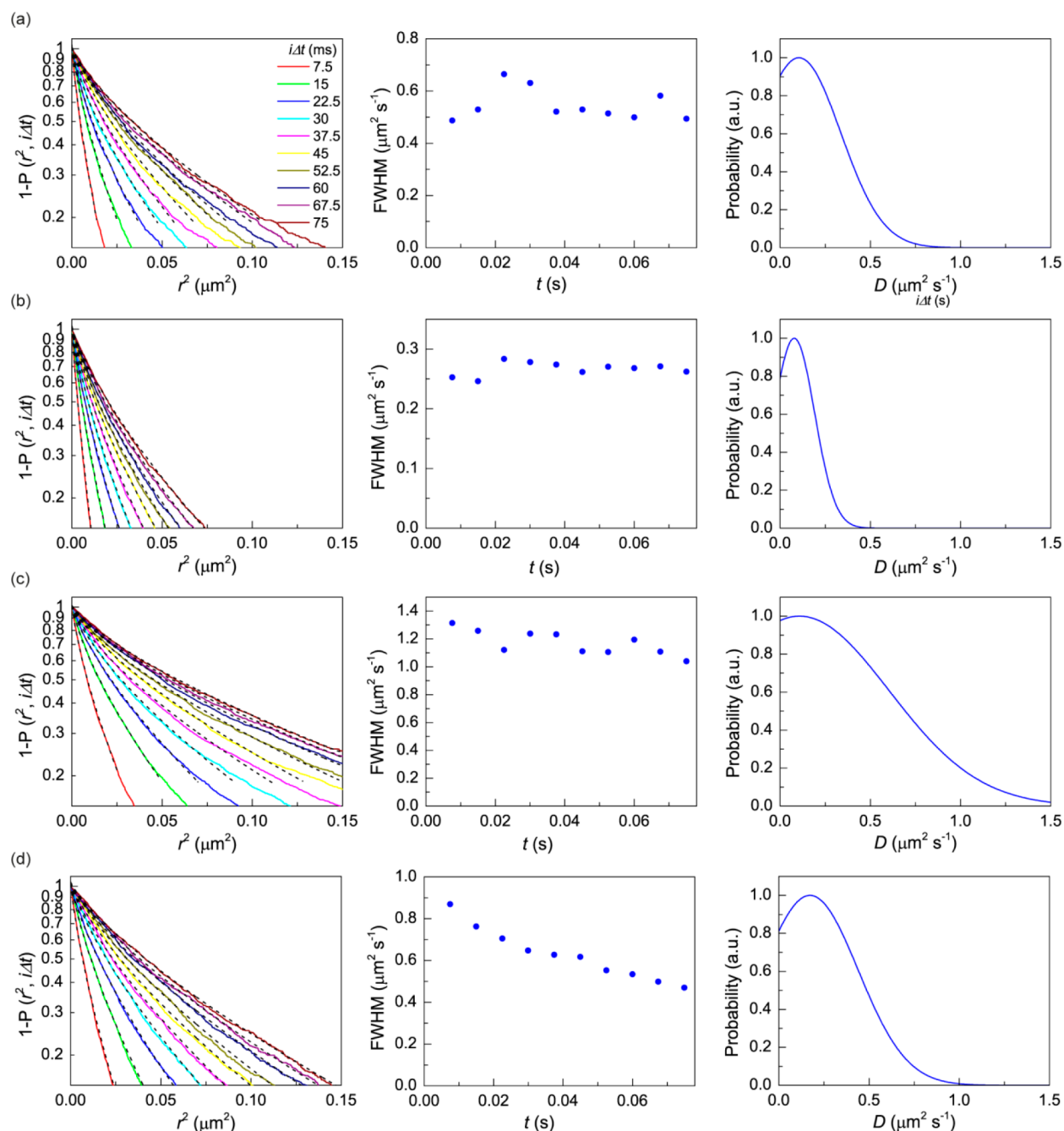


Figure 5. (left) Experimentally obtained cumulative distribution functions ($i\Delta t = 7.5\text{--}75$ ms) in the form of $1-P$ (solid lines) for (a) **1** at 303 K, (b) **2** at 303 K, (c) **1** at 313 K, and (d) **2** at 313 K. Dashed lines show fittings with eq 7. (center) Widths of the distribution of diffusion coefficient determined by the fittings of cumulative distribution functions with eq 7. (right) Statistical distributions of the diffusion coefficient determined by the fittings of cumulative distribution functions with eq 7.

coefficients, we analyzed the CDFs with a model which assume the presence of broad distribution of the D values

$$1 - P(r^2, i\Delta t) = \int_0^\infty f(D) D^{-1} \exp\left[-\frac{r^2}{4D(i\Delta t)}\right] dD \quad (7)$$

$$f(D) = A \exp\left\{-\frac{(D - D_0)^2}{2w^2}\right\} \quad (8)$$

where $f(D)$ is probability distribution of D , which is described by Gaussian. All the CDFs can be fitted well with eqs 7 and 8 (Figure 5, left panels, broken lines). The widths of the D value

distributions at each time lag and the probability distributions of the D values determined from the analysis are shown in Figure 5 (center and right panels, respectively). The statistical probability distribution of D was calculated based on the D value distributions obtained from the CDF analysis using an equation

$$p(D) = \int_0^\infty f(D) \frac{1}{(N-1)!} \left(\frac{N}{D_0}\right)^N (D)^{N-1} \exp\left(-\frac{ND}{D_0}\right) dD \quad (9)$$

where $f(D)$ is probability distribution of D determined by the CDF analysis. The statistical distributions calculated based on eq 9 (Figure 4, green lines) reasonably reproduce the experimentally determined D value histograms. The satisfactorily fitting of the CDFs (Figure 5, left panels) together with the good agreement between the experiments and theory in the D value distributions strongly suggest that both **1** and **2** have broad distributions of the diffusion coefficient in the melt states (see below).

Simulation studies have suggested that both flexible linear and cyclic polymers which have chain lengths similar to **1** and **2** show multiple entanglements with linear chains in the melt.^{58,59} Therefore, it is likely that each polymer chain has a different number of entanglements-threading. In addition, the matrix linear poly(THF)s have a relatively large molecular weight distribution. Although the different number of entanglements-threading and the chain length distribution could be the factors which affect the broad distributions of the diffusion coefficient, the broad distributions of the diffusion coefficient were observed in the length scale of a micrometer and time scale of tens of milliseconds. If the chain interaction is described by the constraint release model, the spatiotemporal heterogeneity of the diffusion coefficient should be averaged out in the length scale of the gyration radius of the chain and in the time scale of the displacement of the chain on the order of its gyration radius. In the present study, the large heterogeneity of the diffusion was observed in a micrometer length scale and tens of milliseconds time scale, which are much larger than the gyration radius of the chain (~ 2 nm) and the displacement time (~ 30 μ s). Therefore, our findings cannot be interpreted by the constraint release model. These results rather indicate the presence of spatiotemporal heterogeneity of the polymer diffusion which occurs at much larger time and length scales than those expected from the current polymer physics theory.

The cyclic polymer (**2**) at 313 K showed a time lag dependence of the D value distribution (Figure 5d, center panel), while the nearly constant D value distributions were observed for the other samples. Although we can only speculate the origin of the time lag dependent D value distribution at the current stage, such behavior could be accounted for by the averaging of the heterogeneous diffusion process on the time scale of tens of milliseconds. The temporal heterogeneity in the diffusion process observed in the present study as well as the spatial heterogeneity of the polymer dynamics found in other studies cannot be fully interpreted by the polymer dynamics theory developed based on ensemble averaged experimental methods. The spatiotemporal heterogeneities of polymer dynamics observed in the single-molecule microscopy studies demonstrate that molecular level understanding of the polymer dynamics requires the methodologies which enable one to analyze the spatiotemporal behavior of individual polymer chains.

Topology Dependent Chain Interaction. The average D of **1** at 303 K (Figure 4a) is 45% larger than that of **2** (Figure 4b). The difference in D between **1** and **2** is much smaller in the semidilute solution (15% at 303 K).⁴⁸ A similar trend (i.e., slower diffusion of the cyclic chain in the linear-cyclic blend as compared with the linear chain in the linear chain matrix) was observed for the naturally occurring DNA in the semidilute solution.²⁹ Those results suggest very efficient threading of **2** with the linear poly(THF)s in the melt. In contrast, relatively inefficient threading of **2** with the linear poly(THF)s in the semidilute solution was suggested by the bimodal distribution

in the D histogram observed in the previous study.⁴⁸ Analysis of the D histogram suggests that roughly 60% of the cyclic chains are threaded by the linear chains in the semidilute solution (see the Supporting Information). An ensemble experiment on the cyclic-linear blend in the melt demonstrated slower diffusion of the cyclic chain as compared with the linear chains in the mixture.³⁰ It has also been suggested by simulation work that the diffusion of the cyclic polymer molecules was significantly slowed by the threading with linear chains.⁶⁰ These studies also support the idea that the efficient threading of **2** with the linear chains occurs in the melt, and as a result the diffusion of **2** slows down.

The average D of **1** and **2** at 313 K (Figure 4c,d) are 1.7 and 1.9 times faster than those at 303 K (Figure 3a,b), respectively. Activation energy of the diffusion (E_D) was calculated from the temperature dependence of D (see the Supporting Information). Although the E_D was determined from the narrow temperature range, **2** showed larger E_D (52 kJ mol⁻¹) as compared with **1** (43 kJ mol⁻¹). Although smaller E_D values have been reported for linear PEO with molecular weights similar to **1** and **2** in the melt by means of NMR spectroscopy (24–26 kJ mol⁻¹),^{61,62} these results were obtained at much higher temperature ranges (344–413 K). The entanglement behavior near the melting temperature (303–313 K) could be significantly different from that at the higher temperature. The simulation study predicts that the linear and cyclic chains with an identical molecular weight have a similar number of entanglement/threading with the linear matrix chains in the melt.⁵⁹ This result suggests that the larger activation energy barrier observed for **2** reflects the diffusion of the threaded chains rather than difference in the number of the entanglements-threading. More detailed single-molecule experiments on the chain length and temperature dependence of the diffusion^{13,63} will provide further information about the complicated molecular mechanism of the cyclic polymer dynamics.

CONCLUSIONS

Polymer physics theories have been developed based on ensemble averaged experimental methods which do not provide direct information about microscopic heterogeneities. The recent development of single-molecule fluorescence microscopy techniques has been revolutionizing the way we study polymer dynamics as they can directly reveal nanoscopic heterogeneities of complicated polymer dynamics. The single-molecule techniques have been revealing spatiotemporal heterogeneity of polymer dynamics which cannot be fully interpreted within the framework of current polymer physics theories. In the present study, we demonstrated the broad distributions of the diffusion coefficient of the polymer chains in the melt state and topology dependent chain interactions in the melts. The single-molecule approaches will further provide insight into the complicated polymer physics and will contribute to the molecular level understanding of polymer dynamics.

ASSOCIATED CONTENT

Supporting Information

Calculation of entanglement number, double-exponential fittings of the CDFs, estimation of threading efficiency in the semidilute solution, and movies of single-molecule diffusion. This material is available free of charge via the Internet at <http://pubs.acs.org>.

■ AUTHOR INFORMATION

Corresponding Author

*E-mail: satoshi.habuchi@kaust.edu.sa (S.H.), ytezuka@o.cc.titech.ac.jp (Y.T.).

Notes

The authors declare no competing financial interest.

■ ACKNOWLEDGMENTS

This work was supported by a Grant-in-Aid for Scientific Research Grant No. 22750122 (S.H.), Grant No. 20340109 (M.V.), Grant No. 23685022 (T.Y.), Grant No. 23106709 (T.Y.), and Grant No. 23350050 (Y.T.) of the Japan Society for the Promotion of Science. S.H. is grateful for the Kurata Grant.

■ REFERENCES

- (1) Gräslund, A.; Rigler, R.; Widengren, J., Eds. *Single Molecule Spectroscopy in Chemistry, Physics and Biology*; Springer: Heidelberg, Germany, 2010.
- (2) Hellriegel, C.; Kirstein, J.; Brauchle, C. *New J. Phys.* **2005**, *7*, 23.
- (3) McCain, K. S.; Hanley, D. C.; Harris, J. M. *Anal. Chem.* **2003**, *75*, 4351–4359.
- (4) Kim, H. B.; Habuchi, S.; Kitamura, N. *Anal. Chem.* **1999**, *71*, 842–848.
- (5) Leger, L.; Hervet, H.; Rondelez, F. *Macromolecules* **1981**, *14*, 1732–1738.
- (6) Klein, J. *Nature* **1978**, *271*, 143–145.
- (7) von Meerwall, E. D.; Amis, E. J.; Ferry, J. D. *Macromolecules* **1985**, *18*, 260–266.
- (8) Bartko, A. P.; Xu, K. W.; Dickson, R. M. *Phys. Rev. Lett.* **2002**, *89*, 026101.
- (9) Uji-i, H.; Melnikov, S. M.; Deres, A.; Bergamini, G.; De Schryver, F.; Herrmann, A.; Mullen, K.; Enderlein, J.; Hofkens, J. *Polymer* **2006**, *47*, 2511–2518.
- (10) Woll, D.; Braeken, E.; Deres, A.; De Schryver, F. C.; Uji-i, H.; Hofkens, J. *Chem. Soc. Rev.* **2009**, *38*, 313–328.
- (11) Deres, A.; Floudas, G. A.; Mullen, K.; Van der Auweraer, M.; De Schryver, F.; Enderlein, J.; Uji-i, H.; Hofkens, J. *Macromolecules* **2011**, *44*, 9703–9709.
- (12) Schob, A.; Cichos, F.; Schuster, J.; von Borczyskowski, C. *Eur. Polym. J.* **2004**, *40*, 1019–1026.
- (13) Flier, B. M. I.; Baier, M.; Huber, J.; Mullen, K.; Mecking, S.; Zumbusch, A.; Woll, D. *Phys. Chem. Chem. Phys.* **2011**, *13*, 1770–1775.
- (14) Flory, P. J. *Principles of Polymer Chemistry*; Cornell University Press: Ithaca, NY, 1953.
- (15) De Gennes, P.-G. *Scaling Concepts in Polymer Physics*; Cornell University Press: Ithaca, NY, 1979.
- (16) Doi, M.; Edwards, S. F., *The Theory of Polymer Dynamics*. Oxford University Press: New York, 1987.
- (17) McLeish, T. C. B. *Adv. Phys.* **2002**, *51*, 1379–1527.
- (18) Rubinstein, M.; Colby, R. H., *Polymer Physics*. Oxford University Press: Oxford, U.K., 2003.
- (19) Perkins, T. T.; Smith, D. E.; Chu, S. *Science* **1994**, *264*, 819–822.
- (20) Smith, D. E.; Perkins, T. T.; Chu, S. *Macromolecules* **1996**, *29*, 1372–1373.
- (21) Kas, J.; Strey, H.; Sackmann, E. *Nature* **1994**, *368*, 226–229.
- (22) McLeish, T. *Science* **2002**, *297*, 2005–2006.
- (23) Brown, S.; Szamel, G. *J. Chem. Phys.* **1998**, *109*, 6184–6192.
- (24) Suzuki, J.; Takano, A.; Deguchi, T.; Matsushita, Y. *J. Chem. Phys.* **2009**, *131*, 144902.
- (25) Hur, K.; Jeong, C.; Winkler, R. G.; Lacevic, N.; Gee, R. H.; Yoon, D. Y. *Macromolecules* **2011**, *44*, 2311–2315.
- (26) Cosgrove, T.; Griffiths, P. C.; Hollingshurst, J.; Richards, R. D. C.; Semlyen, J. A. *Macromolecules* **1992**, *25*, 6761–6764.
- (27) Cosgrove, T.; Turner, M. J.; Griffiths, P. C.; Hollingshurst, J.; Shenton, M. J.; Semlyen, J. A. *Polymer* **1996**, *37*, 1535–1540.
- (28) von Meerwall, E.; Ozisik, R.; Mattice, W. L.; Pfister, P. M. *J. Chem. Phys.* **2003**, *118*, 3867–3873.
- (29) Robertson, R. M.; Smith, D. E. *Proc. Natl. Acad. Sci. U.S.A.* **2007**, *104*, 4824–4827.
- (30) Nam, S.; Leisen, J.; Breedveld, V.; Beckham, H. W. *Macromolecules* **2009**, *42*, 3121–3128.
- (31) Kapnistos, M.; Lang, M.; Vlassopoulos, D.; Pyckhout-Hintzen, W.; Richter, D.; Cho, D.; Chang, T.; Rubinstein, M. *Nat. Mater.* **2008**, *7*, 997–1002.
- (32) Klein, J. *Macromolecules* **1986**, *19*, 105–118.
- (33) Mills, P. J.; Mayer, J. W.; Kramer, E. J.; Hadzioannou, G.; Lutz, P.; Strazielle, C.; Rempp, P.; Kovacs, A. J. *Macromolecules* **1987**, *20*, 513–518.
- (34) McKenna, G. B.; Hostetter, B. J.; Hadjichristidis, N.; Fetters, L. J.; Plazek, D. J. *Macromolecules* **1989**, *22*, 1834–1852.
- (35) Richter, D.; Ewen, B.; Farago, B.; Wagner, T. *Phys. Rev. Lett.* **1989**, *62*, 2140–2143.
- (36) Tead, S. F.; Kramer, E. J.; Hadzioannou, G.; Antonietti, M.; Sillescu, H.; Lutz, P.; Strazielle, C. *Macromolecules* **1992**, *25*, 3942–3947.
- (37) Richter, D.; Willner, L.; Zirkel, A.; Farago, B.; Fetters, L. J.; Huang, J. S. *Phys. Rev. Lett.* **1993**, *71*, 4158–4161.
- (38) Griffiths, P. C.; Stilbs, P.; Yu, G. E.; Booth, C. J. *Phys. Chem.* **1995**, *99*, 16752–16756.
- (39) Nam, S.; Leisen, J.; Breedveld, V.; Beckham, H. W. *Polymer* **2008**, *49*, 5467–5473.
- (40) Milner, S. T.; Newhall, J. D. *Phys. Rev. Lett.* **2010**, *105*, 208302.
- (41) Sakaue, T. *Phys. Rev. Lett.* **2011**, *106*, 167802.
- (42) Muller, M.; Wittmer, J. P.; Cates, M. E. *Phys. Rev. E* **1996**, *53*, 5063–5074.
- (43) Vettorel, T.; Grosberg, A. Y.; Kremer, K. *Phys. Biol.* **2009**, *6*, 025013.
- (44) Freedman, K. O.; Lee, J.; Li, Y. G.; Luo, D.; Skobeleva, V. B.; Ke, P. C. *J. Phys. Chem. B* **2005**, *109*, 9839–9842.
- (45) Muls, B.; Uji-i, H.; Melnikov, S.; Moussa, A.; Verheijen, W.; Soumilion, J. P.; Josemon, J.; Mullen, K.; Hofkens, J. *ChemPhysChem* **2005**, *6*, 2286–2294.
- (46) Gavranovic, G. T.; Csihony, S.; Bowden, N. B.; Hawker, C. J.; Waymouth, R. M.; Moerner, W. E.; Fuller, G. G. *Macromolecules* **2006**, *39*, 8121–8127.
- (47) Aoki, H.; Mori, K.; Ito, S. *Soft Matter* **2012**, *8*, 4390–4395.
- (48) Habuchi, S.; Satoh, N.; Yamamoto, T.; Tezuka, Y.; Vacha, M. *Angew. Chem., Int. Ed.* **2010**, *49*, 1418–1421.
- (49) Vacha, M.; Habuchi, S. *NPG Asia Mater.* **2010**, *2*, 134–142.
- (50) Adachi, K.; Takasugi, H.; Tezuka, Y. *Macromolecules* **2006**, *39*, 5585–5588.
- (51) Oike, H.; Imaizumi, H.; Mouri, T.; Yoshioka, Y.; Uchibori, A.; Tezuka, Y. *J. Am. Chem. Soc.* **2000**, *122*, 9592–9599.
- (52) Yamamoto, T.; Tezuka, Y. *Polym. Chem.* **2011**, *2*, 1930–1941.
- (53) Habuchi, S.; Onda, S.; Vacha, M. *Chem. Commun.* **2009**, 4868–4870.
- (54) Habuchi, S.; Onda, S.; Vacha, M. *Phys. Chem. Chem. Phys.* **2011**, *13*, 1743–1753.
- (55) Nishimura, S. Y.; Lord, S. J.; Klein, L. O.; Willets, K. A.; He, M.; Lu, Z. K.; Twieg, R. J.; Moerner, W. E. *J. Phys. Chem. B* **2006**, *110*, 8151–8157.
- (56) Vrljic, M.; Nishimura, S. Y.; Brasselet, S.; Moerner, W. E.; McConnell, H. M. *Biophys. J.* **2002**, *83*, 2681–2692.
- (57) Schutz, G. J.; Schindler, H.; Schmidt, T. *Biophys. J.* **1997**, *73*, 1073–1080.
- (58) Helfer, C. A.; Xu, G. Q.; Mattice, W. L.; Pugh, C. *Macromolecules* **2003**, *36*, 10071–10078.
- (59) Subramanian, G.; Shanbhag, S. *Phys. Rev. E* **2008**, *77*, 011801.
- (60) Yang, Y. B.; Sun, Z. Y.; Fu, C. L.; An, L. J.; Wang, Z. G. *J. Chem. Phys.* **2010**, *133*, 064901.
- (61) Appel, M.; Fleischer, G. *Macromolecules* **1993**, *26*, 5520–5525.
- (62) Cheng, S. Z. D.; Barley, J. S.; Vonmeerwall, E. D. *J. Polym. Sci., Part B: Polym. Phys.* **1991**, *29*, 515–525.

(63) Flier, B. M. I.; Baier, M. C.; Huber, J.; Mullen, K.; Mecking, S.; Zumbusch, A.; Woll, D. *J. Am. Chem. Soc.* **2012**, *134*, 480–488.